JOURNAL OF MATERIALS SCIENCE 7 (1972) 202–210

Rubber-Toughening of Plastics

Part 1: *Creep Mechanisms in HIPS*

C. B. BUCKNALL, D. CLAYTON
Department of Materials, Cranfield Institute of Technology, Cranfield, Bedford, UK

A new and quantitative method for studying rubber-toughening is presented: the extent of crazing in creep specimens is determined from time-dependent volume changes, which are compared with longitudinal strains in order to determine the contribution of other mechanisms. The results show that creep deformation in HIPS under high tensile stress consists essentially of elastic deformation followed by crazing. A simple model for the kinetics of crazing is developed, from which rate constants for initiation (k_i) and propagation (k_p) of crazes are obtained. Both k_i and k_p exhibit an Eyring-type dependence upon stress, with the same apparent activation volume of 5000 Å^3.

1. Mechanisms of Toughening

There is an increasing need for quantitative methods for studying rubber-toughening in plastics. Qualitative methods have produced some important information on the subject during the past decade, but it is becoming clear that existing methods are inadequate for the detailed studies of relationships between structure and mechanical properties that are now needed. The work presented in the present paper is therefore aimed at the production of deformation data that will yield quantitative information about the mechanisms of rubber-toughening.

The most important existing method for studying toughening mechanisms is microscopy, which is unique in its ability positively to identify specific mechanisms, but is extremely difficult to use quantitatively in determining the contributions of two competing mechanisms to the total deformation. Existing mechanical test methods, which could perhaps be developed to give quantitative information, have so far been used only to distinguish between alternative mechanisms. The information obtained by these qualitative methods is reviewed below.

1.1. Microscopy

Earlier ideas about mechanisms were revised following the work of Bucknall and Smith [1], who used optical microscopy to demonstrate that crazing plays an important part in rubber-toughening, a conclusion that has since been confirmed by electron microscopy [2-4]. At about the same time, Schmitt [5] suggested, also on the basis of optical microscopy, that microcracking also contributes to toughening, but the positive evidence for a significant amount of microcracking, as distinct from crazing, does not appear to be very strong. Furthermore, Kambour [6] has shown that cracking is preceded by crazing in glassy polymers, so that microcracking should be regarded as the final stage of the crazing process, rather than as a distinct mechanism.

An alternative approach to rubber-toughening was proposed by Newman and Strella [7], who concluded from optical microscope studies that cold drawing is responsible for toughness in ABS. More recently, McGarry [8] obtained evidence for both micro-shear bands and crazes in rubber-modified epoxide resins. McGarry's observations are supported by optical and electron microscope evidence obtained by Bucknall *et al* [9] for shear bands and crazes in rubber-modified PPO (poly phenylene oxide).

1.2. Mechanical Tests

The stress field requirements for crazing are quite different from those for cold drawing and shear band formation; Sternstein and Ongchin [10] have shown that crazing follows a stress-

bias criterion that is quite distinct from the Mohr-Coulomb criterion for shear band formation [10, 11]. McGarry and Oien [12] used the difference between the two criteria to study deformation mechanisms in biaxially-loaded specimens of rubber-modified epoxide resin, and concluded that large rubber particles initiate crazes, whereas small rubber particles tend to generate shear bands.

Further evidence for the effect of stress field upon deformation mechanism was obtained by Biglione, Baer, and Radcliffe [13], who showed that hydrostatic pressure suppresses craze formation in ABS and HIPS.

1.3. Evaluation of Previous Work

The results and conclusions outlined above can be summarised in the statement that crazing is the basic mechanism of toughening, and that shear band formation, general cold drawing, and other mechanisms, supplement the contribution of crazing. There is evidence in McGarry's work [12] for a co-operative interaction between crazes and shear bands: greater toughness is achieved when both mechanisms are present than when either is acting alone.

This analysis emphasises the importance of quantitative methods. The problem is not simply to identify a single mechanism of toughening, but to assess the separate contributions of several competing and interacting mechanisms to the total deformation, and to describe the kinetics of each mechanism.

2. A Quantitative Method

The principle of the method presented in this paper is that the extent of craze formation in a specimen under constant load can be measured by following volume increases, and that the contribution of other mechanisms can be determined by comparing volume strain with longitudinal strain. The analysis is based upon the classification of toughening mechanisms under two headings: (i) cavitation mechanisms: crazing, microcracking, and other voiding processes; and (ii) shear yielding mechanisms: shear band formation and general cold drawing.

In equating time-dependent volume increases with crazing, it is assumed (a) that the bulk modulus of uncrazed material does not alter during the test; (b) that shear yielding mechanisms do not contribute significantly to the dilatation; and (c) that cavitation mechanisms other than crazing can be neglected. Assumptions (a) and (b) are supported by dilatation measurements on creep specimens of HIPS under low tensile stress, and of rubber-free polymers, which do not show significant amounts of crazing during the test. Assumption (c) is based upon evidence from microscopy, but must be checked for each material tested.

The experiment outlined above could be carried out in a number of ways. The simplest is a tensile creep test in which length and thickness strains are measured accurately in isotropic specimens. This approach was followed in the present work. A brief preliminary note on the results has been published [14].

3. Experimental Procedure

3.1. Material

Tests were carried out upon HT-91, a HIPS material made by the Monsanto Company. An electron micrograph showing the microstructure of this polymer has been published by Kambour and Russell [4].

3.2. Creep Tests

Sheets of HIPS 2 mm thick were compression-moulded at 180°C. Dumb-bell specimens, with a parallel gauge portion 40 mm long, 5 mm wide, and 2 mm thick, were milled from these sheets.

Eleven specimens were tested in uniaxial tension at stresses σ between 19 and 24 MN m^{-2}, using high-accuracy lever-loading creep rigs designed by Dr M. W. Darlington [15]. The test temperature was 20 $\pm \frac{1}{2}$°C. Longitudinal strain e_3 was measured in the central 20 mm of the specimen. Thickness strain e_1 was measured simultaneously, at the centre of the gauge portion, and the volume strain $\Delta V/V$ was calculated as $(e_3 + 2e_1)$; e_1 is, of course, usually negative in a tensile test.

Each long-term creep test was preceded by a loading-unloading programme at successively increasing loads, in order to obtain a 100 sec isochronous curve of modulus against 100 sec strain, within the low strain region [16]. During this preliminary programme, stress levels were kept well below those used for long-term testing. Long-term tests were terminated when e_3 reached a value of about 5 %, when the specimen was unloaded and allowed to recover. The loading-unloading programme was then repeated, in order to obtain another 100 sec isochronous curve, showing the effects of creep history upon the HIPS. Details of the isochro-

nous and recovery curves will be published in a later paper.

3.3. Microscopy

Strained creep specimens were sectioned parallel to the tensile axis, microtomed to produce a flat surface, and etched using the method of Bucknall, Drinkwater, and Keast [9]. This technique enables both rubber particles and crazes to be observed under the optical microscope. Photomicrographs were made of representative areas within the gauge portion.

4. Results

4.1. Basic Creep Data

Isochronous creep curves of 100 sec modulus against 100 sec strain show that at short times the HIPS is a linear viscoelastic solid at strains below about 0.2 %, but becomes distinctly non-linear as the strain rises towards 1.0 %; there is a 10 % drop in modulus over this range.

Fig. 1 shows long-term creep results, plotted as longitudinal creep compliance J_3 against $\log(t)$, where $J_3 = e_3/\sigma$, and t = time. Creep rates are highly dependent upon σ, but the

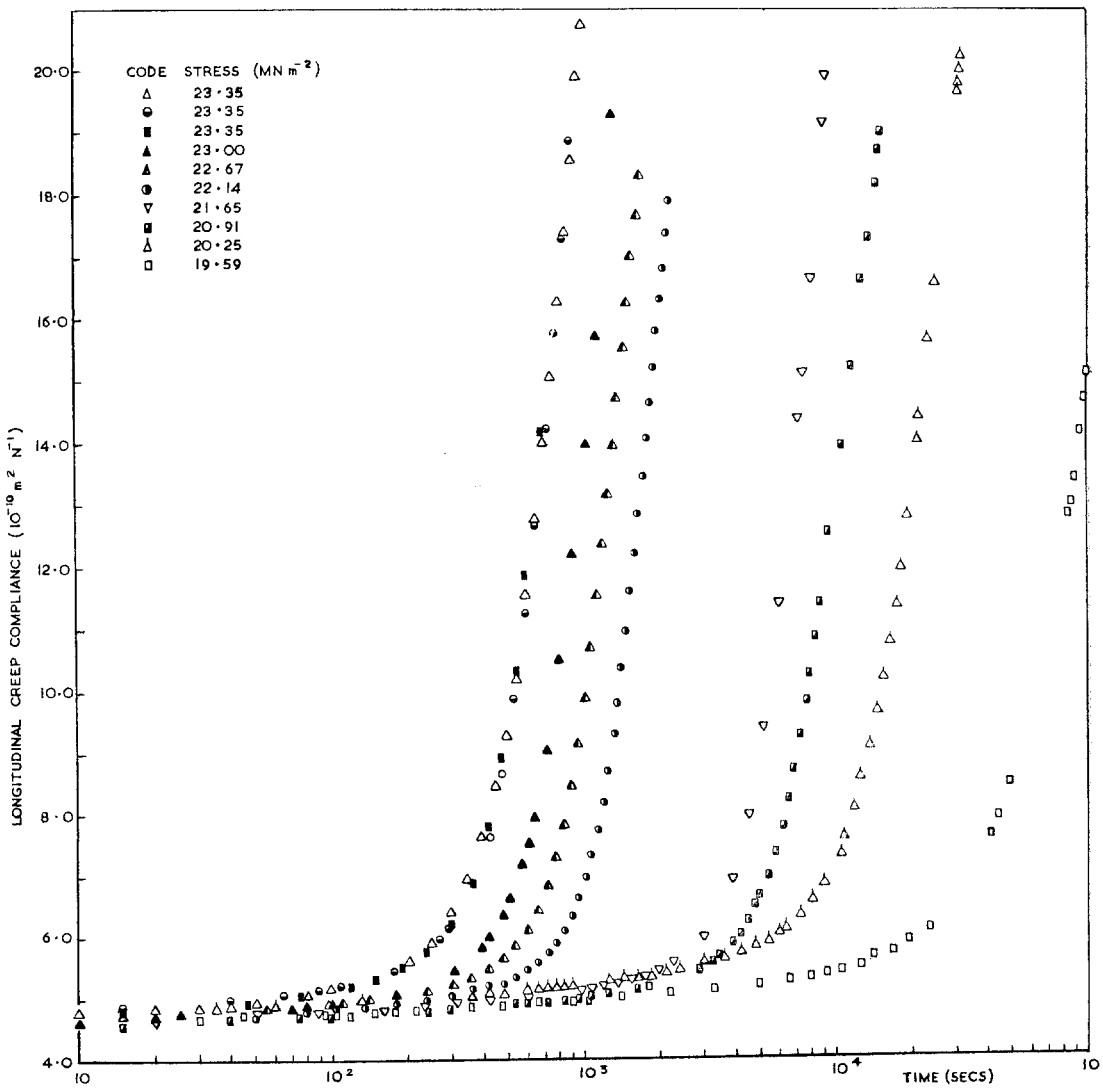

Figure 1 Longitudinal creep compliance J_3 versus time t for isotropic HT-91 HIPS at high stresses.

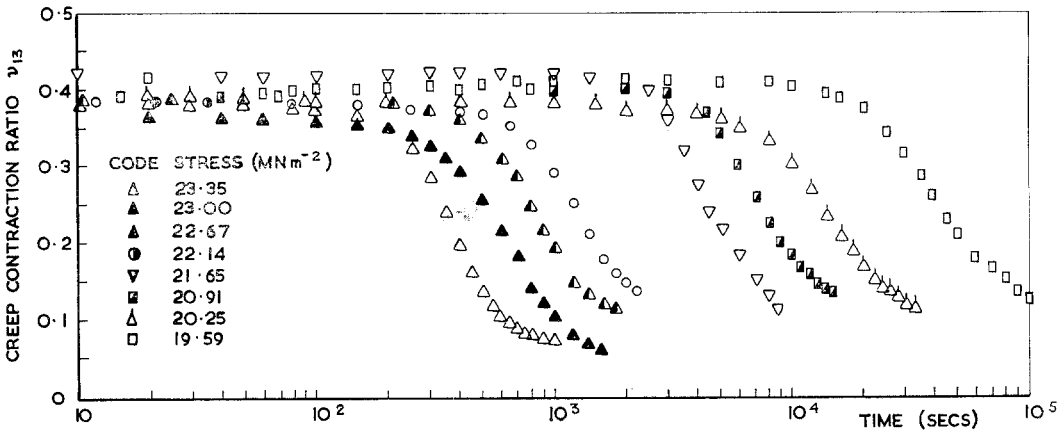

Figure 2 Creep contraction ratio ν_{13} versus t; specimens as in fig. 1.

form of the curves is the same in all cases: there is an instantaneous elastic response to the applied stress, followed by a slow but accelerating deformation, which is accompanied by a slight whitening of the specimen, indicating that the material is crazing; finally, the creep rate becomes high, and the whitening becomes very pronounced.

Fig. 2 shows corresponding values of creep contraction ratio ν_{13} ($= -e_1/e_3$). The instantaneous value of ν_{13} is about 0.4, and there is comparatively little change during the slow stage of the creep deformation. At the beginning of the rapid-creep stage, ν_{13} begins to fall, finally reaching a value of less than 0.1. The main reason for this fall is the rapid increase in e_3, but there is a small additional effect: the magnitude of e_1 shows a temporary decrease during this period, indicating a slight thickening of specimen. Talysurf studies of surface contours show that the effect is due to the formation of minute bulges approximately 1 μm high on the surface in densely-crazed areas; the bulges disappear when the specimen is unloaded.

4.2. Volume Changes

Figs. 3 and 4 show how the volume of the HIPS increases with time. The dilatation can be divided into three stages, which correspond exactly with the three stages discussed in the previous section:

(i) Instantaneous dilatation; due to the ordinary elastic response to hydrostatic tension.

(ii) Slow dilatation; due to crazing. The rate of dilatation increases throughout this stage.

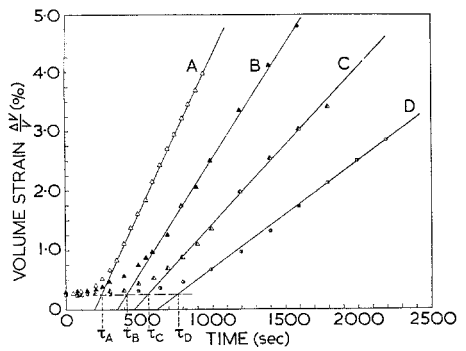

Figure 3 Volume strain $\Delta P/V$ versus t at four stress levels: (a) 23.35; (b) 23.00; (c) 22.67; and (d) 22.14 MN m^{-2}.

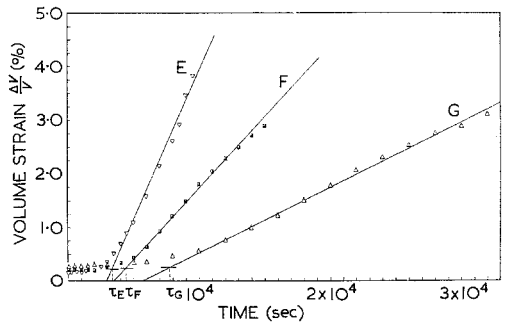

Figure 4 Volume strain $\Delta V/V$ versus t at three stress levels: (a) 21.65; (f) 20.91; and (g) 20.25 MN m^{-2}.

(iii) Rapid dilatation; also due to crazing. The rate of dilatation has a constant high value $[\mathrm{d}(\Delta V/V)/\mathrm{d}t]_{\max}$ throughout this stage.

We have given the name "induction period" to stage (ii), and defined its duration τ as shown

in figs. 3 and 4: the linear portion of each curve is extrapolated back to the point at which the volume strain is equal to instantaneous volume strain. The induction period is the time interval required for the attainment of an appreciable rate, as in the case of a chemical reaction.

The curves of volume strain against time define two rate quantities:
(*a*) the final rate of dilatation, $[\mathrm{d}(\Delta V/V)/\mathrm{d}t]_{\max}$; and
(*b*) the reciprocal induction time τ^{-1}. The significance of these quantities is discussed in section 5.3.

4.3. Accuracy

The ultimate limitation upon the accuracy of the measurements was imposed by the transducers and associated recording equipment, which have a limit of resolution of 1 μm in the measurement of deflection.

The curves of 100 sec isochronous modulus against 100 sec strain for the eleven specimens tested provided a practical test of the accuracy of the strain measurements. At $e_3 = 0.001$, the scatter in e_3 was less than 3 %, and the scatter in e_1 was less than 12 %. At $e_3 = 0.01$, the corresponding figures were 1 % scatter in e_3 and 5 % in e_1.

As another check of accuracy, four specimens were subjected to long term creep tests at a single stress level of 23.35 MN m^{-2}. Within the induction period, the reproducibility was better than 1 % for e_3, and better than 5 % for e_1. Beyond the induction period, the bulging effect discussed in section 4.1 increases the scatter in e_1 to approximately 30 %. However, e_3 is unaffected by the bulging phenomenon, and the errors in e_1 have little effect upon the calculated volume strain, which is largely determined by e_3 during this stage of creep.

4.4. Microscopy

Fig. 5 is an optical micrograph of a crazed region in a creep specimen that was unloaded at a strain of 5.0 %. The etched surface shown was microtomed parallel to the tensile stress, and therefore normal to the plane of the crazes. The rubber component appears in the form of spherical particles between 1 and 5 μm in diameter. The crazes are roughly parallel, between 1 and 10 μm long, and about 2 μm apart, on average. There is little evidence for shear bands or other deformation mechanisms than crazing.

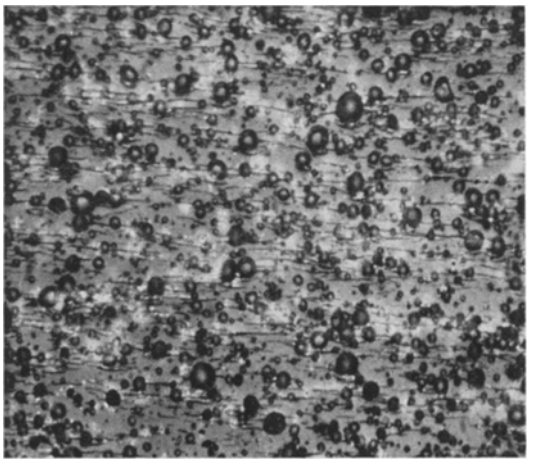

Figure 5 Optical micrograph showing rubber particles and crazes in HIPS after creep test to 5% strain. Stress direction vertical. Microtomed block etched in chromic acid [3]. Magnification: × 650.

5. Discussion

5.1. Relative Importance of Crazing

The results presented in section 4 show clearly that tensile creep in the HIPS used for this work consists essentially of an instantaneous elastic deformation, followed by crazing. Specimens were unloaded at longitudinal strains e_3 of 5 %, and this figure can be divided approximately as follows: instantaneous elastic strain 1.1 %; shear yielding processes and time-dependent elastic deformation 0.1 %; crazing 3.8 %. The figure of 0.1 % for shear yielding and viscoelastic effects is estimated from the lateral contraction strain e_1, which exhibits a general downward trend (specimen contracting) throughout the test, although there is a temporary increase in e_1 for most specimens at one point during the test, owing to the slight bulging noted in section 4.1.

The ratio of volume strain ($\Delta V/V$) to longitudinal strain e_3 provides a convenient form for expressing the contribution of crazing to the total elongation. This ratio, which we have called the dilatation factor ϕ, is plotted against e_3 in fig. 6. The dilatation factor ϕ is related to creep contraction ratio ν_{13} as follows

$$\phi = \frac{\Delta V}{V} \Big/ e_3 = (e_3 + 2e_1)/e_3 = 1 - 2\nu_{13}$$

Thus ϕ is zero for an imcompressible material ($\nu = 0.5$), and 1.0 for a material deforming entirely by craze or crack opening, without

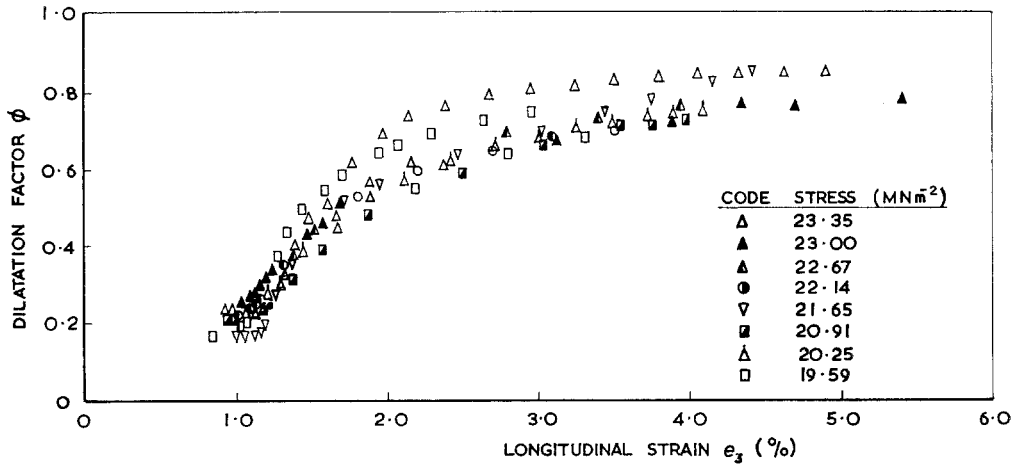

Figure 6 Dilatation factor ϕ versus longitudinal strain e_3 for HIPS.

lateral contraction. Fig. 6 provides support for the suggestion made by previous authors, that crazing should be considered as a strain-controlled process.

The value of ϕ is about 0·2 in the low-strain region ($e_3 < 1.0$; $\nu_{13} \simeq 0.4$), where elastic deformation is the dominant mechanism. As e_3 rises above 1.0 %, ϕ rises towards 1.0, reflecting the increasing importance of crazing. However, the maximum value attained by ϕ within the strain range of the test is 0.85, because the deviatoric elastic strain contributes significantly to e_3 when e_3 is of the order of 5 % or less.

5.2. Kinetics of Crazing

We propose a simple model for the kinetics of crazing in HIPS, as a first step towards interpreting our results. The model includes several simplifying assumptions, which might require modification in the light of later knowledge. Nevertheless, the model is a valuable aid in understanding the creep results, and in suggesting further experiments.

The model is based upon three assumptions, relating to the initiation, propagation, and termination of crazes at a constant stress σ:
(*a*) That the number of crazes N formed per unit volume of polymer is proportional to the time t under load.

$$N = k_I t \tag{1}$$

where k_I is the rate constant for craze initiation.
(*b*) That the craze tip advances at a constant rate.

$$dr/dt = k_P \tag{2}$$

where r is a linear dimension of the craze, i.e. its length or radius, and k_P is the rate constant for craze propagation.
(*c*) That the craze ceases to propagate when it reaches a certain size, owing to a collision with rubber particles in its path, or other similar processes. The average limiting size of crazes will be determined by the spacing between rubber particles, but will be independent of stress and temperature.

Writing $\bar{V}$ for the average contribution per craze to the increase in volume of the specimen, i.e. the difference between the volume of the craze and the volume of the bulk polymer from which it was formed, we obtain the following expression for volume strain:

$$\Delta V/V = N\bar{V} = k_I \bar{V} t \tag{3}$$

whence:

$$\frac{d}{dt}\left(\frac{\Delta V}{V}\right) = k_I \bar{V} + k_I t \frac{d\bar{V}}{dt} \tag{4}$$

Expressions for $\bar{V}$ are obtained by a treatment similar to that developed by Avrami [17] for crystallisation in polymers. Two cases are considered below: unidirection growth of a rectangular plate, and radial growth of a disc-shaped craze.

5.2.1. Unidirectional Growth Model

Consider a rectangular craze of constant thickness, h, constant width w, and length r, where r increases with time, according to equation 2. If the craze was initiated at time θ, and has a void content of g, the additional contribution V

of the craze to the volume of the specimen is given by:

$$V = ghwr = ghw\, k_P\, (t - \theta)$$

Since the fraction of crazes formed in the time interval $d\theta$ is $d\theta/t$, the average volume contribution $\bar{V}$ per craze is given by:

$$\bar{V} = \int_{\theta=0}^{t} ghw\, k_P\, (t - \theta)\, \frac{d\theta}{t}$$

$$= \tfrac{1}{2}\, ghw\, k_P\, t$$

Substituting into (3) we obtain:

$$\Delta V/V = (\tfrac{1}{2}\, ghw\, k_I\, k_P)t^2 \qquad (5)$$

5.2.2. Disc Model

In this model, the craze is considered as a circular disc of constant thickness h and radius r, where r increases with time, according to equation 2. The treatment is similar to that presented in section 5.2.1:

$$V = \pi\, r^2\, gh = \pi\, k_P^2\, gh\, (t - \theta)^2$$

$$\therefore\ \bar{V} = \int_0^t \pi\, k_P^2\, gh\, (t - \theta)^2\, \frac{d\theta}{t}$$

$$= \frac{\pi}{3}\, gh\, k_P^2\, t^2$$

Substituting into (3) this gives:

$$\Delta V/V = \left(\frac{\pi}{3}\, gh\, k_I\, k_P^2\right)t^3 \qquad (6)$$

5.2.3. Comparison with Experiment

An examination of the experimental results shows that the time-dependent component of volume strain, i.e. the contribution due to crazing, increases as the square rather than the cube of time during the slow stage of creep. In other words, equation 5 provides the best description of the creep behaviour during the induction period.

During the subsequent rapid stage of creep, the rate of dilatation is constant, and the deformation can be represented by equation 4, provided that $\bar{V}$ is taken as constant. This condition is fulfilled if the number of terminated crazes is much greater than the number of propagating crazes, so that $\bar{V}$ is the average volume contribution of a craze at termination:

$$\bar{V} = ghwR$$

where R is the average length of the crazes at termination. Substituting into (4) we obtain:

$$d(\Delta V/V)/dt = k_I\, (ghwR) \text{ at } t > \tau \qquad (7)$$

5.2.4. Rate Constants k_I and k_P

Since R can be considered as a materials constant, independent of stress and temperature, and the stress range of the experiment is insufficient to affect g,h, and w significantly, it follows from equation 7 that the increase in $[d(\Delta V]V)/dt_{max}$ with stress is directly proportional to the increase in k_I with stress. Furthermore, the absolute magnitude of k_I can be estimated by substituting reasonable values for g,h,w, and R into equation 7. Taking g as 0.5 and h, w and R as 0.1, 2.0 and 5.0 μm respectively, we obtain a value of 10^{-4} crazes per cubic micron per second for k_I at a stress of 23.00 MN m^{-2}.

The propagation rate constant k_P is inversely proportional to the induction period τ, which represents the time at which the first crazes formed reach the point of termination; since from equation 2:

$$r = k_P t \text{ for the first crazes}$$

$$\text{whence: } k_P = \frac{R}{\tau} \text{ at termination} \qquad (8)$$

Taking $R = 5.0$ μm as before, we obtain a value of 0.02 μm/sec for k_P at a stress of 23.00 MN m^{-2}.

5.3. Eyring Rate Theory

In fig. 7, the two characteristic rate quantities $[d(\Delta V/V)/dt]_{max}$. and τ^{-1} are plotted on a logarithmic scale against the applied stress σ. Two parallel straight lines are obtained, indicating that both rate quantities follow the Eyring rate equation [18, 19]:

Rate $= 2A \sinh(\gamma v\sigma/kT) \simeq A \exp(\gamma v\sigma/kT)$

where A = constant, γ = stress concentration factor, v = activation volume, k = Boltzmann's constant, T = temperature.

The slope of the lines corresponds to a value of approximately 5000 Å^3 for the apparent activation volume γv. From equations 7 and 8 we conclude that the quantities plotted in fig. 7 are effectively k_I and k_P, and that the activation volume obtained should be regarded as the activation volume for craze formation. Since craze propagation proceeds through a secondary initiation process, of void formation in a region of high stress concentration, it is not altogether surprising that the apparent activation volume is the same for initiation as for propagation.

In the present case, the increases in volume

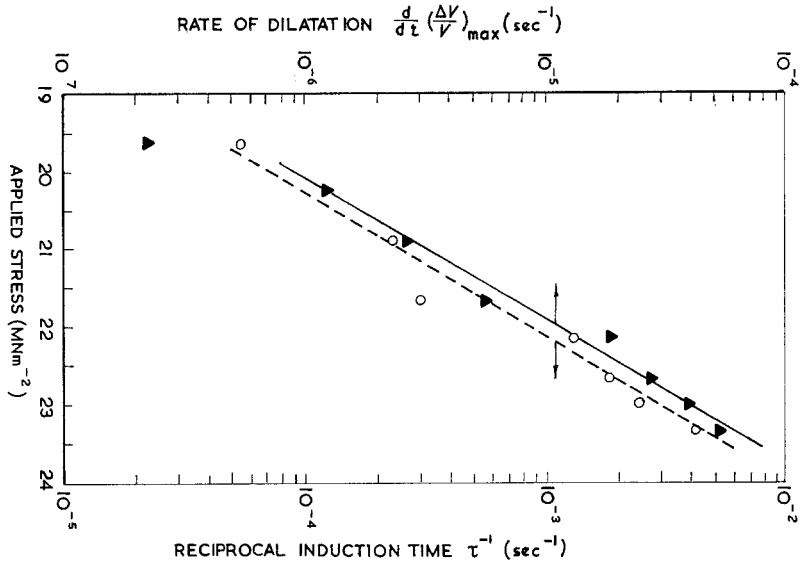

Figure 7 Eyring plots of rate of dilatation $\frac{d}{dt}\left(\frac{\Delta V}{V_{max}}\right)$ and reciprocal induction time τ^{-1} versus applied stress.

strain and longitudinal strain are almost equivalent, especially at higher strains, because the time-dependent part of the deformation is almost entirely due to crazing. Consequently, an Eyring plot of longitudinal strain rate would be equally meaningful. However, this is not generally true for rubber-modified polymers. For example, the creep of ABS includes a major contribution from both crazing and shear deformation processes, and the rate of elongation is therefore a composite quantity, determined by at least two contrasting deformation mechanisms.

5.4. Tests at Constant Strain Rate

The creep tests show that under constant tensile stress, the strain rate in HIPS increases with strain until a limiting rate is reached. The corollary of this statement is that under constant strain rate conditions, the stress decreases with strain until it reaches a limiting stress level. In other words, there is a fall in true stress beyond the yield point in a conventional tensile test.

The yield drop, which is well known, can now be understood in terms of craze formation. The stress rises initially, to initiate a large number of crazes, and then falls as these crazes grow, because a lower stress is required to produce the same rate of crazing.

5.5. Limitations of Model

The simple model presented in section 5.2 cannot be applied without modification to all rubber-toughened polymers. Experiments upon grades of rubber-toughened plastics other than HT-91 HIPS show that the kinetics of crazing can deviate in a number of ways from the simple model. In some materials, especially those containing very small rubber particles, the rate of crazing continues to increase throughout the test, instead of levelling out at the end of an induction period; this behaviour suggests that the craze termination mechanism is less effective in these materials. In other materials, the rate of crazing decreases throughout the test, suggesting that additional craze-terminating features are formed under stress. Details of these experiments will be published in later papers.

6. Conclusions

On the basis of these experiments, we conclude that creep deformation at comparatively high stresses in the test material, a typical HIPS polymer, consists essentially of two components, an instantaneous elastic component, and crazing. The kinetics of crazing can be described by a simple model based upon the Avrami treatment, from which rate constants for craze initiation and propagation can be evaluated. Both rate constants fit the Eyring equation.

The dilatometric method described in this paper is clearly a powerful technique for studying rubber-toughening, and analysing the mechanisms contributing to toughness. However, the implications of this work are wider. The results provide an insight into the whole field of deformation and failure mechanisms in glassy polymers.

Acknowledgements

The authors thank the Science Research Council for a grant in support of this work, and Mrs Wendy Keast for assistance with microscopy.

References

1. C. B. BUCKNALL and R. R. SMITH, *Polymer* **6** (1965). 437.
2. M. MATSUO, *ibid*, **7** (1966) 421.
3. *Idem, Polymer Eng. Sci.* **9** (1969) 206.
4. R. P. KAMBOUR and R. R. RUSSELL, *Polymer* **12** (1971) 237.
5. J. A. SCHMITT, *J. Appl. Polymer Sci.* **12** (1965) 533.
6. R. P. KAMBOUR, *J. Polymer Sci.* **A2 4** (1966) 17.
7. S. NEWMAN and S. STRELLA, *J. Appl. Polymer Sci.* **9** (1965) 2297.
8. F. J. MCGARRY, *Proc. Roy. Soc.* **A319** (1970) 59.
9. C. B. BUCKNALL, I. C. DRINKWATER, and W. KEAST, *Polymer* in press.
10. S. S. STERNSTEIN and L. ONGCHIN, ACS Polymer Preprints, **10** (2) (1969) 1117.
11. P. B. BOWDEN and J. A. JUKES, *J. Mater. Sci.* **3** (1968) 183.
12. F. J. MCGARRY and H. M. OIEN, private communication.
13. G. BIGLIONE, E. BAER, and S. V. RADCLIFFE, Proceedings of the Second International Conference on Fracture (Chapman and Hall, London, 1969).
14. C. B. BUCKNALL and D. CLAYTON, *Nature* (*Phys. Sci.*) **231** (22), (1971) 107.
15. M. W. DARLINGTON and D. W. SAUNDERS, *J. Phys.* **E 3** (1970) 511.
16. S. TURNER, *Trans. J. Plastics Inst.* **31** 60 (1963).
17. M. GORDON, High Polymers (2nd edn.), (Iliffe, London, 1963) 126.
18. W. KAUZMANN, *Trans. Amer. Inst. Min. Met. Eng.* **143** (1941) 57.
19. R. N. HAWARD and G. THACKRAY, *Proc. Roy. Soc.* **A302** (1968) 453.

Received 16 August and accepted 7 September 1971.